A plasticity and damage model for fiber reinforced polymers

Ulrich Hofer

University of Innsbruck, Austria

Abstract: The Abaqus damage model for fiber reinforced plastics has been reimplemented as UMAT user material. As an extension, the plastic behavior of the matrix material is taken into account. Therefore, two modes are considered independently from each other: matrix shear and matrix compression. The original as well as the new material model have been verified by means of single element tests, mesh dependency tests, and the standard plate-with-a-hole problem. In addition, a shell-type structure, namely an industrial model of the Boeing-777 Winglet, has been analyzed.

Keywords: Composites, Constitutive Model, Progressive Damage, Plasticity, Polymer, User Material.

1. Introduction

The role of composite materials has become more important in the last decades, since they are very important in areas in which lightweight structures are used, for example in the aerospace or automotive industry. An important class of composites consists of two materials, namely a fiber with excellent tensile strength and stiffness properties and a matrix with poor mechanical properties (Michaeli, 1994).

The aim of this paper, based on (Hofer, 2012), is to describe the constitutive behavior of composite materials. For this purpose, a user subroutine UMAT is written, which takes into account anisotropy and brittle damage behavior as well as irreversible strains remaining after unloading, formulated in terms of plane stress. A plasticity model, which considers plastic strain only under transversal compression and shear as described in (Flatscher, 2009), was coupled with a brittle damage model as presented in (Lapczyk, 2007).

2. Damage model

A damage model as described in (Abaqus Analysis, 2009) has been reimplemented as a UMAT User subroutine.

The strength of a material is characterized by six parameters: X_t and X_c denote the tension resp. compression strength of the fiber, Y_t and Y_c the tension resp. compression strength of the matrix, S_l and S_t denote the longitudinal and transversal shear strength. There are four different failure modes to consider: Fiber tension, fiber compression, matrix tension and matrix compression.

The same failure initiation criteria as in Abaqus, which are based on the Hashin initiation criteria, have been implemented in the user subroutine; the influence of the shear stress to the failure mode “fiber tension” has been neglected. The failure criteria are formulated in terms of effective stress

$$\sigma_{ef} = \mathbf{M}\sigma, \tag{1}$$

where σ is the nominal stress, σ_{ef} the effective stress and **M** is the damage operator:

$$\mathbf{M} = \begin{pmatrix} \frac{1}{1-d^{\mathrm{f}}} & 0 & 0 \\ 0 & \frac{1}{1-d^{\mathrm{m}}} & 0 \\ 0 & 0 & \frac{1}{1-d^{s}} \end{pmatrix}. \tag{2}$$

Here, d^{f} , d^{m} and d^{s} denote fiber, matrix and shear damage variables. Note that the shear damage variable is not independent, because it is obtained from fiber and matrix damage. For a virgin material, the effective stress is equal the nominal stress, while at fracture, $\sigma_{ef} \rightarrow \infty$.

It should be noted that Abaqus uses a different definition for the effective shear stress for the evaluation of the damage initiation criteria. These definitions depend on the respective damage initiation criterion, for which the effective shear stress is calculated:

$$\sigma_{12,eff}^{crit} = \sigma_{12} \frac{(1-d^{ft})(1-d^{fc})(1-d^{mt})(1-d^{mc})}{(1-d^{s})(1-d^{crit})}. \tag{3}$$

The index “crit” denotes one of the four damage initiation criteria (“ft”, “fc”, “mt” or “mc”), the indices “f” resp. “m” denote fiber respective matrix, the indices “t” resp. “c” denote tension resp. compression damage. This distinction in the definition of the effective shear stress has not been made in the UMAT subroutine, so that slight differences can be observed in the results between Abaqus and User subroutine (see Section 4).

After a damage criterion is exceeded, the material stiffness begins to degrade. It is assumed that the evolution of the damage variables only depends on the fracture energy *G*. The damage at a time step n+1 is approximated by a hyperbolic function of the equivalent displacement δ_{eq}:

$$d_{n+1} = max\left(\frac{\delta_{eq,n+1}^{f}\left(\delta_{eq,n+1}-\delta_{eq,n+1}^{0}\right)}{\delta_{eq,n+1}\left(\delta_{eq,n+1}^{f}-\delta_{eq,n+1}^{0}\right)}, d_{n}\right). \tag{4}$$

It is shown in Figure 1.a. Here, δ_{eq}^{0} is the equivalent displacement when damage occurred the first time and δ_{eq}^{f} is the equivalent displacement at complete failure of the material, referring to the corresponding failure mode.

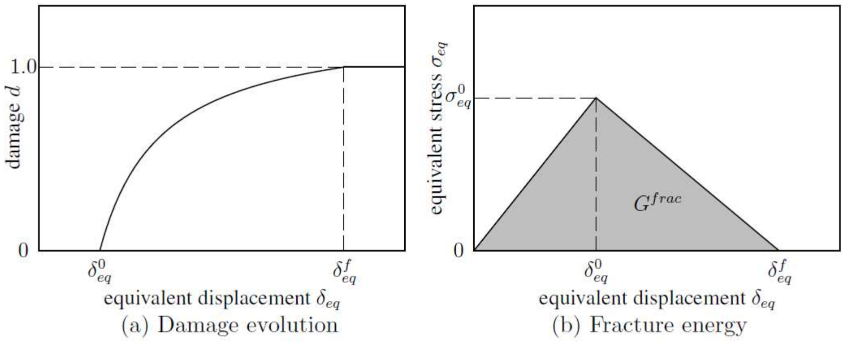

Figure 1. Evolution of damage and equivalent stress.

In Figure 1.b, σ_{eq}^{0} is the equivalent stress, when a failure criterion is reached the first time. In this figure it can also be seen that the area under the function equals the fracture energy, which is the total energy dissipated in turn of complete rupture. So the equivalent displacement at complete failure, δ_{eq}^{f}, is not a material parameter. It depends on the fracture energy G, which is a material parameter, and on the equivalent stress σ_{eq}^{0}. δ_{eq}^{f} can then be computed from the area of the triangle (Figure 1.b):

$$\delta_{eq}^{f} = 2\mathrm{G}/\sigma_{eq}^{0}. \tag{5}$$

For the calculations of the equivalent displacement at first failure it is assumed that all stress components increase in the same ratio to each other; σ_{eq}^{0} is then calculated following (Lapczyk, 2007) for all four failure modes. If all four damage variables (for fiber tension resp. compression and matrix tension resp. compression) are computed, the dependent shear damage variable is calculated as proposed in (Lapczyk, 2007):

$$d^{s} = 1 - (1 - d^{ft})(1 - d^{fc})(1 - d^{mt})(1 - d^{mc}). \tag{6}$$

The updated stress tensor is calculated using the damaged stiffness tensor

$$\mathbf{C}^{d} = \frac{1}{\mathrm{D}}\begin{pmatrix} (1-d^{f})\mathrm{E}_{11} & (1-d^{f})(1-d^{m})\nu_{21}\mathrm{E}_{22} & 0 \\ (1-d^{f})(1-d^{m})\nu_{12}\mathrm{E}_{11} & (1-d^{m})\mathrm{E}_{22} & 0 \\ 0 & 0 & \mathrm{D}(1-d^{s})\mathrm{G}_{12} \end{pmatrix} \tag{7}$$

with $D = 1 - (1 - d^f)(1 - d^m)\nu_{12}\nu_{21}$.

To avoid convergence problems and mesh dependent solutions, a viscous regularization scheme has to be introduced:

$$\dot{d}^v = {}^1\!/_\eta\,(d - d^v). \tag{8}$$

Integrating the above differential equation with the backward Euler method yields

$$d_{n+1}^v = \left(\frac{\eta}{\eta+h}\right) d_n^v + \left(\frac{h}{\eta+h}\right) d_{n+1}. \tag{9}$$

Here, the index "v" denotes the viscous damage variable, h is the time step and η is the viscosity parameter. It can easily be seen that if the viscosity parameter is small compared to the time increment, the viscous solution converges to the inviscid one.

Consequently, the value of the viscosity parameter η should be chosen as large as needed for convergence but as small as possible to ensure that the viscosity has not a big influence on the solution of the computations.

To achieve a quadratic convergence rate in the global Newton iterations, a consistent tangent operator for the damaged material has been derived. For this purpose, the material law $\sigma_i = \mathrm{C}_{\mathrm{ik}}^{\mathrm{d}}\varepsilon_{\mathrm{k}}$ is differentiated:

$$\frac{\partial\sigma_i}{\partial\varepsilon_j} = \frac{\partial \mathrm{C}_{ik}^d}{\partial\varepsilon_j}\varepsilon_k + \mathrm{C}_{ik}^d\frac{\partial\varepsilon_k}{\partial\varepsilon_j} = \frac{\partial \mathrm{C}_{ik}^d}{\partial\varepsilon_j}\varepsilon_k + \mathrm{C}_{ij}^d. \tag{10}$$

Substituting all differentiations leads finally to

$$\frac{\partial\boldsymbol{\sigma}}{\partial\boldsymbol{\varepsilon}} = \mathbf{C}^{\mathrm{d}} + \boldsymbol{\varepsilon}\colon \sum_{\mathbf{i}} \frac{\partial \mathbf{C}^d}{\partial d_i^v}\frac{\partial d_i^v}{\partial d_i}\frac{\partial d_i}{\partial\boldsymbol{\varepsilon}}, \quad i = [fiber, matrix]. \tag{11}$$

3. Coupled plasticity-damage

Experimental investigations have shown that composites can exhibit plastic behavior (Hobbiebrunken, 2007), (Van Paepegem, 2006) as well as brittle damage behavior. These facts suggest to develop constitutive laws which consider plastic deformations as well as brittle behavior. Such constitutive laws can be obtained by coupling plasticity and damage models, where the plastic models describe the unrecoverable deformations, if a material is yielding, and the damage models describe the different behavior in loading and unloading, if a material is damaged (Ibrahimbegovic, 2009).

In the presented model, two different plasticity mechanisms are assumed: plastic strains driven by shear forces (Mode I) and plastic strains driven by transverse compression (Mode II). In order to keep the needed material parameters, as for example stress interaction parameters or nonlinear hardening parameters, small, the implementation was kept as simple as possible. To keep the computational effort low (to avoid a local iteration scheme), interactions between the two yield modes have not been taken into account.

The damage model remains the same as described in the previous section. After computing the damage model, the plasticity model is activated.

The yield functions Φ for the two modes simply read:

$$\Phi_I = |\sigma_{12}| - \sigma_{y,I} \qquad \Phi_I = -\sigma_{22} - \sigma_{y,II}, \tag{12}$$

where the indices n+1, indicating the current time step, have been omitted for convenience; σ_y denotes the actual yield stress.

A linear hardening law is assumed for the development of the yield thresholds:

$$\sigma_{y,I} = \sigma_{y,I}^0 + \mathrm{C}_I \kappa_I \qquad \sigma_{y,II} = \sigma_{y,II}^0 + \mathrm{C}_{II} \kappa_{II}. \tag{13}$$

Here $\sigma_{y,I,II}^0$ are the initial yield stresses, $\mathrm{C}_{\mathrm{I,II}}$ are the slopes of the linear hardening functions and $\kappa_{I,II}$ are the hardening variables; their rates are defined as

$$\dot{\kappa_I} = |\dot{\gamma}_{12}^p| \qquad \dot{\kappa_{II}} = |\dot{\varepsilon}_{22}^p| \,. \tag{14}$$

The elastic law for a damaged material, the additive split of the strain tensor and the non-associative flow rules

$$\dot{\gamma}_{12}^p = \dot{\lambda}_I \operatorname{sign}(\sigma_{12}) \qquad \dot{\varepsilon}_{22}^p = -\dot{\lambda}_{II} \tag{15}$$

are used to yield expressions for the plastic multiplier:

$$\dot{\lambda}_I = \frac{(1-d^s)\mathrm{G}_{12}}{(1-d^s)\mathrm{G}_{12}+\mathrm{C_I}} \operatorname{sign}(\sigma_{12})\dot{\gamma}_{12} \qquad \dot{\lambda}_{II} = -\frac{\overline{\mathrm{E}}_1\dot{\varepsilon}_{11}+\overline{\mathrm{E}}_2\dot{\varepsilon}_{22}}{\mathrm{C_I}+\overline{\mathrm{E}}_2}, \tag{16}$$

with

$$\overline{\mathrm{E}}_1 = \frac{(1-d^f)(1-d^m)\nu_{12}\mathrm{E}_2}{1-(1-d^f)(1-d^m)\nu_{12}\nu_{21}} \qquad \mathit{and} \qquad \overline{\mathrm{E}}_2 = \frac{(1-d^m)\mathrm{E}_2}{1-(1-d^f)(1-d^m)\nu_{12}\nu_{21}}. \tag{17}$$

With these values of the plastic multiplier, the plastic strains and the internal hardening variables can be calculated for the current time increment.

4. Numerical examples

The damage model without plasticity has been verified and compared to the damage model implemented in Abaqus. For this purpose, single element tests have been made using S4 elements. Displacements have been applied in positive and negative direction, longitudinal and transversal to the fiber direction, respectively. For all four damage modes, the internal Abaqus model and the user subroutine produce the same results regarding load-displacement relations and comparing the energy output (viscous dissipated energy, energy dissipated by damage and elastic strain energy).

As the implemented model is mesh sensitive, also the mesh dependence has been checked. It turned out that the mesh sensitivity strongly depends on the viscosity parameter η: for small values of η (compared to the time increment) the solution converges with increasing mesh refinement. For a larger viscosity parameter the solutions seem not to converge.

Also the standard plate-with-a-hole benchmark test has been made: The example from (Abaqus Example Problems, 2009) has been calculated using the UMAT subroutine. In general, the results have been reproduced well, except deviations in integration points in which more than one damage modes are active. This is because of the different definitions of the effective stress in UMAT and Abaqus as mentioned in Section 2.

As a shell-type structure, an industrial model of the Boeing-777 winglet has been analyzed. Winglets are often attached to the ends of wings of airplanes to reduce the aerodynamic resistance and so to save fuel. The winglet of the Boeing-777 is partially made of composite materials: the upper skin, the lower skin and two spars are built up of several layers of composite materials. Other parts, as the windbox, which connects the winglet with the wing and the leading edge are built of metals. In Figure 2 the meshed composite parts of the winglet can be seen.

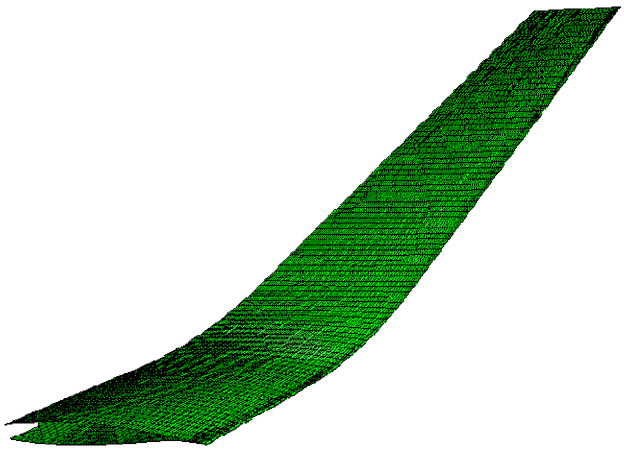

Figure 2. Meshed winglet, composite parts.

The elastic constants and the strength properties are listed in Table 1 and Table 2:

Table 1. Elastic constants of the B-777 composites.

$E_1[lb/in^2]$	$E_2[lb/in^2]$	$\nu[-]$	$G_{12}[lb/in^2]$	$G_{23}[lb/in^2]$	$G_{31}[lb/in^2]$
$8.1 * 10^6$	$8.1 * 10^6$	0.06	$7.0 * 10^5$	$7.0 * 10^5$	$7.0 * 10^5$

Table 2. Strength properties of the B-777 composites.

$X_t[lb/in^2]$	$X_c[lb/in^2]$	$Y_t[lb/in^2]$	$Y_c[lb/in^2]$	$S_l[lb/in^2]$	$S_t[lb/in^2]$
34470	34470	34470	34470	17235	17235

The fracture energy is assumed to be G = 2000 [lb/in] for all failure modes, in the absence of experimental values.

The evolution of the damage variables in some highly damaged integration points has been plotted in Figure 3 –Figure 5:

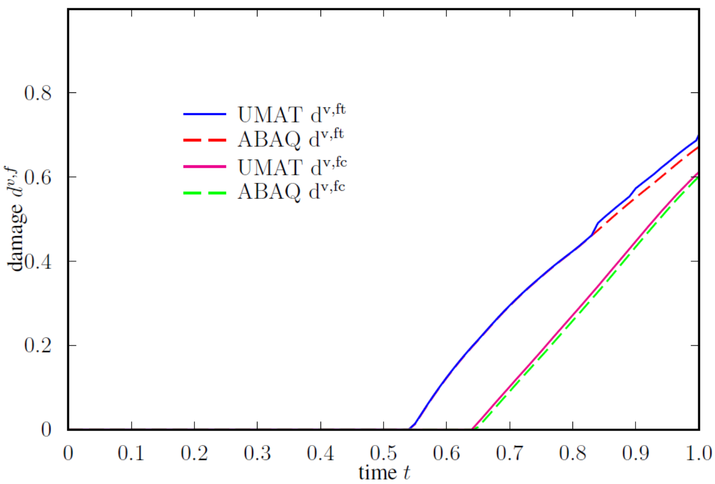

Figure 3. Evolution of fiber damage variables.

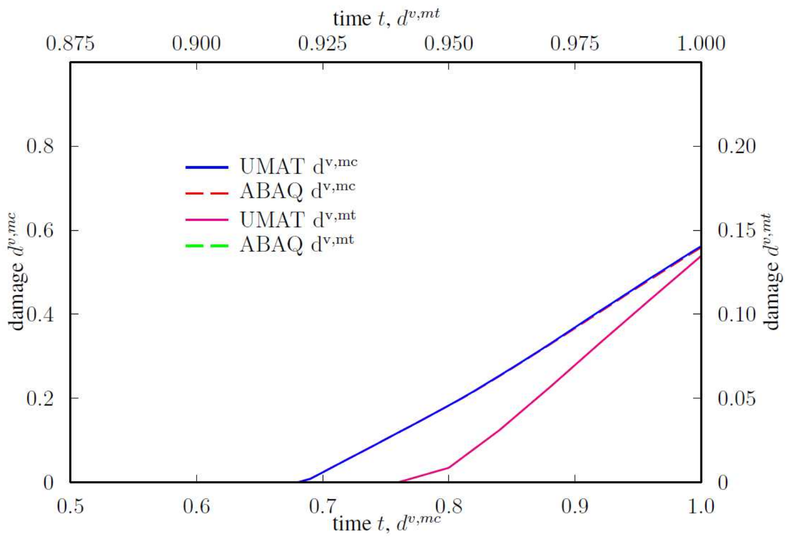

Figure 4. Evolution of matrix damage variables.

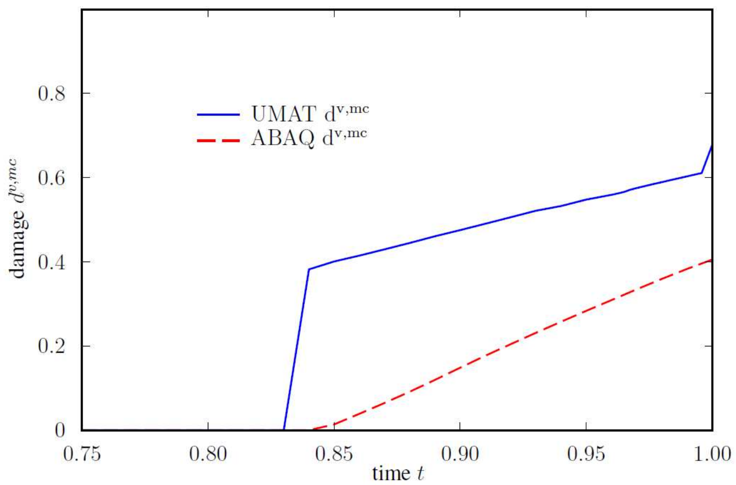

Figure 5. Evolution of matrix compression damage variables.

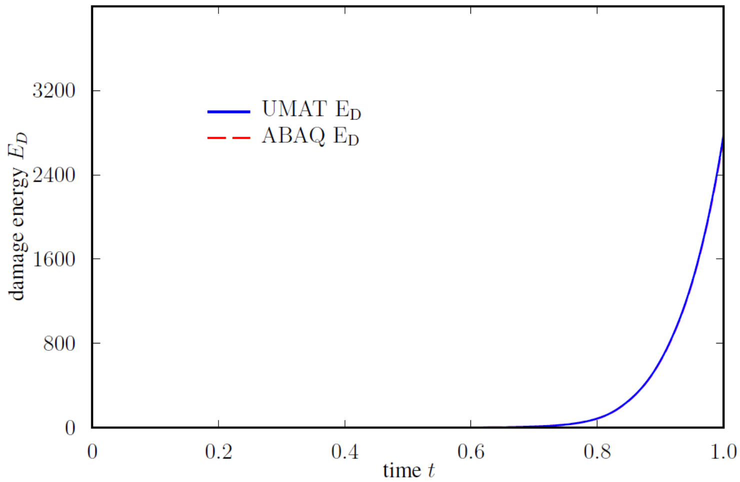

Figure 6. Energy dissipated by damage.

It can be seen that both calculations bring the same results for most cases, so in Figure 6 the total energy dissipated by damage in the whole model is plotted, where both models show good coincidence; also the evolution of damage variables coincides for the most cases. If in an integration point more than one damage mode is active at one time, then there are significant differences, as can be seen in Figure 5. In this integration point, first fiber tension damage occurred and then matrix compression damage. In this case, Abaqus and UMAT arrive at different results. The reason for the deviations is the same as mentioned above in the context of the plate-with-a-hole test.

The coupled plasticity-damage model has been tested at a plate with a hole. Due to its symmetry, only a quarter of it was modeled, which can be seen in Figure 7. It consists only of composite layers, which are listed in Table 7. The mechanical properties are taken from (Lapczyk, 2007), while the yield values are assumed to be slightly smaller than the damage thresholds, see Table 3 – Table 6.

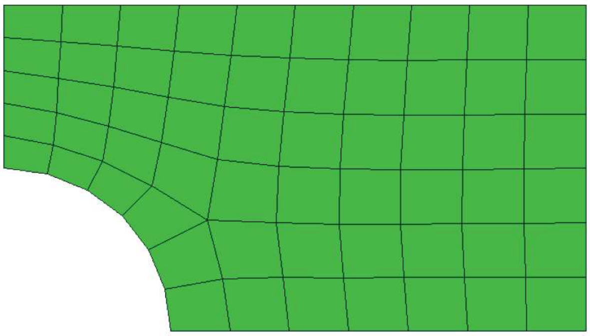

Figure 7. Meshed plate with hole.

Table 3. Elastic constants, plate with hole.

$E_1[N/mm^2]$	$E_2[N/mm^2]$	$G_{12}[N/mm^2]$	$G_{23}[N/mm^2]$	$G_{31}[N/mm^2]$	$\nu_{12}[-]$
55000	9500	5500	3000	5500	0.33

Table 4. Strength properties, plate with hole.

$X_t[N/mm^2]$	$X_c[N/mm^2]$	$Y_t[N/mm^2]$	$Y_c[N/mm^2]$	$S_l[N/mm^2]$	$S_t[N/mm^2]$
2500	2000	50	150	50	50

Table 5. Fracture energies, plate with hole.

$G_{ft}[N/mm]$	$G_{fc}[N/mm]$	$G_{mt}[N/mm]$	$G_{mc}[N/mm]$
12.5	12.5	1	1

Table 6. Plastic properties, plate with hole.

$\sigma_{22}^y[N/mm^2]$	$\tau_{12}^y[N/mm^2]$	$C_I[-]$	$C_{II}[-]$
45	25.98	1000	1000

Table 7. Layer composition, plate with hole.

Number:	#1	#2	#3	#4	#5	#6	#7
Ply angle [°]:	0	80	24	56.4	24	80	0
Ply thickness [mm]:	0.1	0.1	0.1	0.4	0.1	0.1	0.1

For an integration point in the left lower corner, where damage occurs, the stress strain-diagrams have been evaluated (see Figure 8 and Figure 9). In Figure 10 the evolution of the stress variables with respect to time can be seen as well as the evolution of the damage variables d^{mt}(matrix tension damage) and d^{mc}(matrix compression damage).

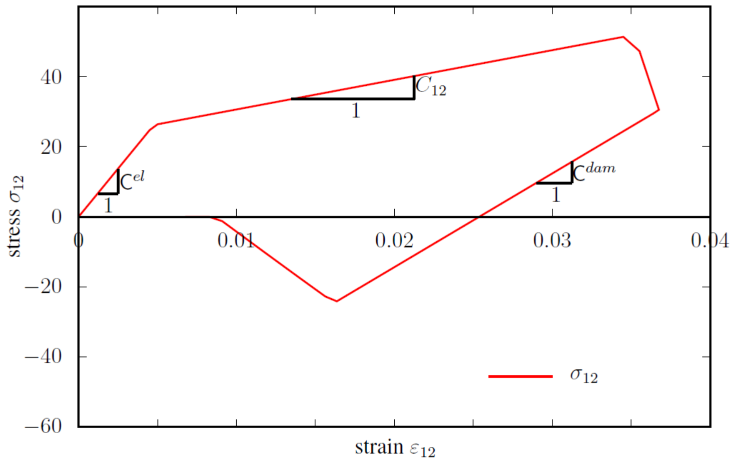

Figure 8. Shear stress-strain diagram.

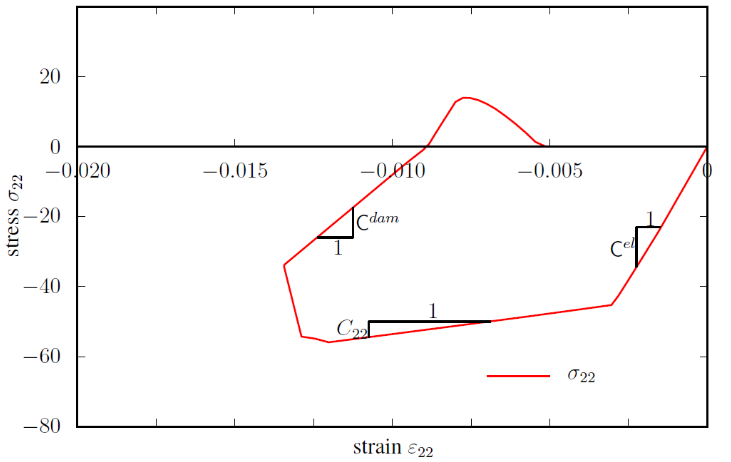

Figure 9. Transverse stress-strain diagram.

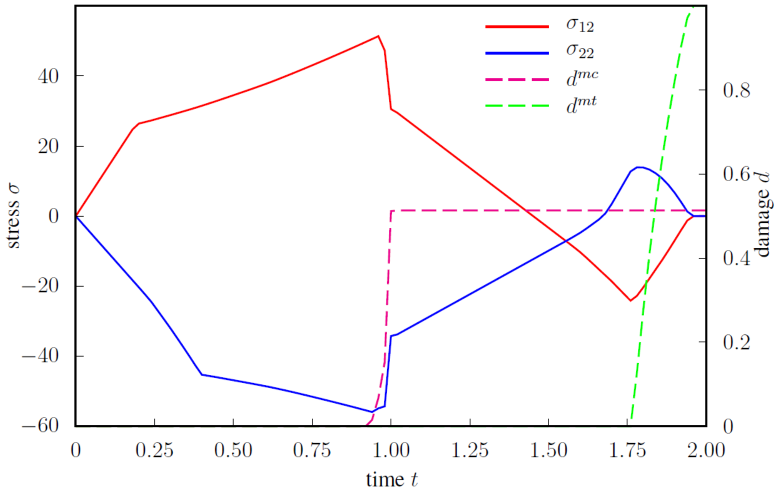

Figure 10. Evolution of stress and damage.

It can be seen in the stress-strain diagrams that at the beginning of loading the stress response is linearly elastic. Then yielding occurs, and the curves show a distinct yield range, before brittle damage occurs (here matrix compression damage) and the nominal stresses decrease. The unloading path is, as expected, not parallel to the loading path, because the proportionality factor is not the initial stiffness as during loading, but the degraded one, following the slope of the damaged stiffness tensor. After complete unloading, the stresses take their opposite sign, until the opposite damage mode (in this case matrix tension damage) is active, and the stresses decrease again until zero, so the material is completely damaged regarding the matrix tension mode. As can easily be seen, permanent (plastic) strains remain after unloading.

5. Conclusions

A UMAT user subroutine has been written, which takes into account plastic as well as brittle behavior. The damage model as well as the coupled plasticity-damage model have been verified by numerical tests: The damage model has been tested using single element tests, mesh dependence tests, the plate-with-a-hole benchmark test and an industrial model of the Boeing-777 Winglet. The original Abaqus model and the UMAT subroutine show good coincidence.

The coupled model has been verified by means of the plate-with-a-hole problem, where the results show the expected behavior. For a wider application, a consistent tangent for the coupled plasticity-damage model should be derived to ensure a quadratic convergence rate during the global Newton-Raphson iterations.

6. References

1. Abaqus. *Version 6.9 Analysis User's Manual.* Providence, RI: Dassault Systèmes Simulia Corp., 2009.
2. Abaqus. *Version 6.9 Example Problems Manual.* Providence, RI: Dassault Systèmes Simulia Corp., 2009.
3. Flatscher, Th., C. Schuecker, and H.E. Pettermann. "Prediction of plastic strain accumulation in continuous fiber reinforced laminates by a constitutive ply model." *International Journal of Fracture*, 2009: 158:145-156.
4. Hobbiebrunken, B., B. Fiedler, M. Hojo, and M. Tanaka. "Experimental determination of the true epoxy resin strength using micro-scaled specimens." *Composites Part A: Applied Science and Manufacturing*, 2007: 38:814:818.
5. Hofer, U. *Plasticity and Damage Models for Fiber Reinforced Polymers.* Diploma thesis. Leopold-Franzens-Universität Innsbruck, 2012.
6. Ibrahimbegovic, A. *Nonlinear solid mechanics: Theoretical Formulations and Finite Element Solution Methods (Solid mechanics and Its Applications).* Dordrecht: Springer, 2009.
7. Lapczyk, I., and J.A. Hurtado. "Progressive damage modeling in fiber-reinforced materials." *Composites Part A: Applied Science and Manufacturing*, 2007: 38(11): 2333-2341.
8. Michaeli, W., D. Huybrechts, and M. Wegener. *Dimensionieren mit Faserverbundkunststoffen.* München: Carl Hanser, 1994.
9. Van Paepegem, W., I. De Baere, and J. Degrieck. "Modelling the nonlinear shear stress-strain response of glass-reinforced composites. Part I: Experimental results." *Composites Science and Technology*, 2006: 66:1455-1464.